**Journal of Emerging Technologies and Industrial Applications**
*Vol. 2 No. 1 (2023) pp. 1-10*
*e-ISSN: 2948-507X*

*Journal homepage: www.mbot.com/jetia*

# CFD Analysis on the Aerodynamic Characteristics of Small-Sized Car Vehicles Under the Influence of Steady Crosswind

**Lim Wei Chen[1], Izuan Amin Ishak[1]***

[1]Centre of Automotive and Powertrain Technology, Faculty of Engineering Technology, Universiti Tun Hussein Onn Malaysia, 84600 Pagoh, Johor, MALAYSIA

Email: izuan@uthm.edu.my

**Abstract:** One of the factors that can cause road accidents is the crosswind. Crosswind is defined as the side force which causes a vehicle to be unstable and allow the vehicle to deviate from its desired path. This article is focusing on assessing the flow behaviour and aerodynamic loads that affect vehicle stability when the car is moving under the influence of steady crosswind. In this study, a numerical approach is performed in which ANSYS Fluent software is utilized as a platform to run the simulation. In this research, the crosswind flow angle ($\Psi$) is varied from 0° to 90°. The incompressible flow surrounding the vehicle is solved using the Reynolds-averaged Navier-Stokes (RANS) equations in conjunctions with the $k$ - $\varepsilon$ turbulence model. The Reynolds number is utilised depending on the velocity of the vehicle which are $2.76\times10^6$ for high Reynolds number and $7.23\times10^5$ for low Reynolds number respectively. In the results, it was found that the crosswind has a significant impact on the aerodynamics quantitatively and qualitatively. In term of aerodynamics load, as the crosswind yaw angle increase, the side coefficient ($C_s$) increases as well. When the crosswind yaw angle ($\Psi$) increases to 60°, it occurs a significant drop then remain almost constant when crosswind yaw angle is at 90°. In flow structure perspective, when the crosswind yaw angle increase, the vortex formation on the leeward region becomes larger, hence increase the imbalance of vehicle stability. Lastly, there is no substantial difference between the aerodynamics quantitative characteristics of the high Reynold number and the low Reynold number.



Received 18 February 2023; Accepted 10 May 2023; Available online 22 June 2023

Keywords: Aerodynamic characteristics, Car vehicle, Flow structure, Steady Crosswind

*Corresponding Author:

Izuan Amin Ishak
Faculty of Mechanical and Manufacturing Engineering,
Universiti Tun Hussein Onn Malaysia, MALAYSIA
Email:

## 1. Introduction

Human introduces vehicles is to allow people to get a shield from wind, rain, and dust when people travel in a car [1]. Road vehicles today play an important role in society. The presence of road vehicles provides numerous advantages in the presence of economical field and environmental fields. In the economical field for instant, it basically will boost the automotive industry and create more job opportunities. Moreover, the advance of technology can produce vehicles such as the electric vehicle (EV) which is fully powered by the electric system, and it will not bring harm to the environment. Even though the presence of the vehicles brings a lot of conveniences, but it had its bad impact. The most concern issue that reflects the bad impact on the vehicles in the accident. The vehicle accident situation may occur anytime and anywhere such as highways, narrow roads, and so on. The most significant accident that may occur due to the transport demand and unsafe operation [2]. The transport demand is concerned about the type of traffic exposure like a high volume of traffic and traffic congestion feature. However, the unsafe operation is concerned with riskier vehicle operation including the driver, vehicle condition, road, and environmental factors [2]. Based on Zulhadi *et al.*, Coleman & Baker and Zhang's studies [2],[3],[4], strong wind is one of the factors that alert the safety of all road users.

When the natural wind is coupled with the direction of traffic, it is referred to as a headwind, crosswind, or tailwind [2]. Headwinds and tailwinds primarily impact longitudinal vehicle speed by pushing back or forward, they do not pose a substantial safety danger [2]. Unfortunately, the crosswind will reflect more impact on the vehicle. Besides, there are two types of crosswind effects on vehicle performance which are crosswind aerodynamic and crosswind stabilities [4]. The crosswind aerodynamics emphasized the relevance of time-related changes in the aerodynamic forces operating on vehicles, which solely focused on the influence of the crosswind on the aerodynamic forces and flow field surrounding the vehicle [4]. Unfortunately, the domination of the aerodynamics force on vehicle performance is largely neglected. The crosswind stability attention is about the vehicle motion and dynamic response under the influence of crosswind. This impact became more significant on the vehicle which has the characteristic of a large flat surface and high center of gravity (COG) [2]. Crosswind flows affect vehicle stability, cornering, and wind noise [5]. In the past, studies on the influence of crosswinds were first conducted on heavy ground vehicles [6]. The heavy grounded vehicles such as trains, trucks, and buses since their vast lateral surfaces render them particularly vulnerable to the impacts of crosswind gusts [5]. Besides, the influence of crosswind can be particularly damaging to heavy trucks. As a result, the improvement in the automotive aerodynamics characteristic alters the researcher's attentiveness to study the influence of crosswinds on light vehicles such as passenger cars [6]. Overturning and the sideslip is the most common situation that influences by the crosswinds to the car vehicle [7].

In terms of stability and control, these vehicles are extremely vulnerable to the effects of crosswinds. The aerodynamics of the vehicle became an important factor that needs to be considered. The different classifications of the vehicle will reflect the varied aerodynamics characteristics depending on the speed of the automobiles and the crosswind angles. High energy losses and the decrease in vehicle performance have resulted from the faster acceleration of vehicle systems. This will have a considerably greater impact when the automobile is driving at high speeds in a crosswind [2]. The relationship between the wind speed and the vehicle's speed can be described as directly proportional to each other where the faster the vehicle, the higher the wind force created [2].

Several numerical investigations regarding the influence of crosswinds on a car vehicle have been carried out in the past. In the study by Bayraktar *et al.* and Tunay *et al* [6],[8], they attended the issue of the crosswind on the flow around the Ahmed vehicle model. The force components acting on the model, the results of the pressure in vertical symmetry plane, instant velocity streamlines and the result of tuft flow visualize. Besides, Millan *et al.* and Tunay *et al* [6],[9] has an experiment to determine the characterization effect of the crosswinds on the drag force ($C_d$) acting on the Ahmed model. The Ahmed vehicle model has a slant angle of $\alpha = 25°$ with a wide range of yaw angles where the range of the yaw angle is from $0° \leq \beta \leq 90°$. From the result of the experiment, it can be discussed that there had three different regions for the drag coefficient ($C_d$) as a role function of the yaw angle $\beta$. The first region is the of the yaw angle $\beta$ was $0° \leq \beta \leq 60°$. This will cause the drag coefficient ($C_d$) to be increased. The second region is the of the yaw angle β was $60° \leq \beta \leq 75°$. This will yield the drag coefficient ($C_d$) to remain constant. Lastly, the third region is where the yaw angle $\beta$ at 90°, and this will alter the drag coefficient ($C_d$) to increase again. Next, in the study by Keogh *et al*. [10], the Ahmed vehicle model had been implied to investigate the impacts on cornering which produce side winds acting on the vehicles. The investigation works with a steady state of constant radius corner where the car length radius corner was set at 5 m, 10 m, and 20 m to model the cornering action. From the result of that investigation, the 5-car length radius corner had an increase of 19.2% in the aerodynamics drag coefficient ($C_d$), followed by 10 and lastly was 20 [10]. Lastly, in the investigation by Meile *et al*.[11], the Ahmed vehicle model had been used to study the effect of the crosswinds at various yaw angles. The range of the various yaw angle is from $-25° \leq \beta \leq 25°$. In the experiment, two slant angles were performed which were the $\alpha = 25°$ and $\alpha = 35°$. From the result of the experiment, it can be deduced that the slant angle at $\alpha = 35°$ alters a more sensitivity to yawing effects than the slant angle at $\alpha = 25°$. The aerodynamics forces and moment are in the range of $10° \leq \beta \leq 15°$ for $\alpha = 35°$.

In the context of a vehicle geometry, according to the past research, the model that had been applied is known as a simplified model where the model does not include the features like side mirror, exhaust, tyre rotational motion and door handles [12]. This article has been arranged as follows. Section 2 goes through the computational setup which includes the model description, grid independence test, size of the enclosure, and boundary condition. Section 3 is described the analysis of the study which evaluates the behaviour of aerodynamics characteristics. Lastly, the summary is made in the article final part.

## 2. **Methods**

### 2.1 **Model Description**

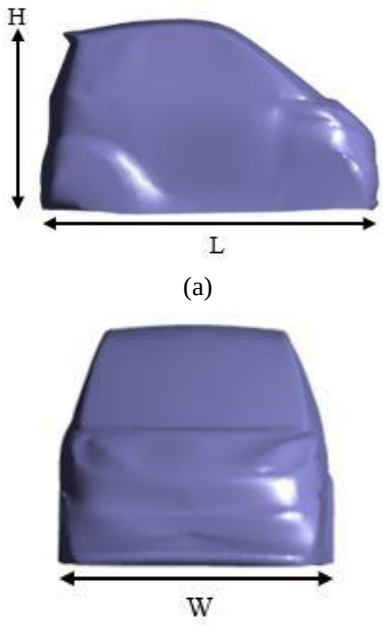


**Fig. 1: Basic shape of the small-sized car**

The type of simplified vehicle model utilized in this is an A-segment vehicle. Figures 1 (a) and (b) show the detailed geometry of the vehicle model. This vehicle can be considered as a small vehicle and the dimension of this car is shown in Table 1. The vehicle model of segment A is imported and modified in SOLIDWORKS, before being transferred to ANSYS Design Modeller. Due to modelling methodology constraints, such as avoiding the influence of rotational motion and tire wake, the tires and exterior parts are ignored.

**Table 1: General dimennsion of the small-sized car vehicle**

| Configuration of the car model | Dimensions (mm) |
|---|---|
| Length | 2403 |
| Width | 1596 |
| Height | 1390 |

## 2.2 Grid Independent Test

An important requirement in the early stages of developing a competent numerical approach was determining an acceptable grid structure with numerical boundary conditions and a turbulence model for numerical simulation [13]. For such purpose, a segment A vehicle with no crosswind condition was chosen and six variations of curvature normal angles had been created with high mesh resolution. Table 2 below shows the high-quality mesh and different curvature normal angles.

**Table 2: The high-quality mesh and different curvature normal angles**

| Curvature normal angles (°) | 18 | 15 | 12 | 9 | 6 | 3 |
|---|---|---|---|---|---|---|
| Number of Nodes | 57,137 | 61,486 | 67,407 | 75,118 | 86,134 | 105,031 |
| Drag Coefficient ($C_d$) | 0.30 | 0.29 | 0.29 | 0.29 | 0.29 | 0.29 |

The inlet velocity that had been applied was the high Reynold number which was $2.73 \times 10^6$. Numerous efforts were made to build a distinctive foundation mesh based on different curvature normal angles. The drag coefficient value ($C_d$) was 0.29 for this segment A vehicle according to the data that had been obtained from the simulation. The graph of drag coefficient ($C_d$) against the number of nodes had been plotted and shown in Figure 2. Based on the result of grid-independent test, the number of nodes 61,486 had been chosen to carry out the real case simulation. This is because at the number of nodes of 61,486 had achieved the convergence of the drag coefficient ($C_d$).

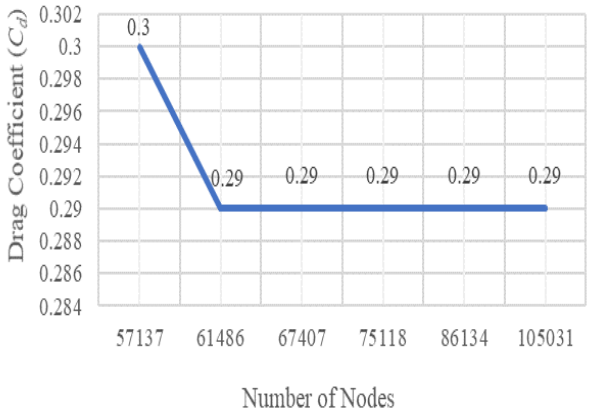


**Fig. 2: Graph of drag coefficient (Cd) against different mesh resolutions**

## 2.3 Steps Performing Ansys Simulation

The first step to perform the Ansys simulation is to construct a 3D model before the simulation runs. A 3D model is imported from SOLIDWORKS into ANSYS within this project. The creation of the model is generated in ANSYS, and the fluid domain is created prior to the meshing phase. The computational domain or the enclosure is defined as the airflow simulation at the confined area. This is to confirm the flow simulation that inside the enclosure boundary will happen and occur. Fundamental parameters on the distances of the length between the inlet and the vehicle, the outlet, and the vehicle for the validation case are based on the latest

studies[12], [14], [15]. Before proceeding to the meshing process, the enclosure must be effective enough to ensure the computational domain is at its ideal size. The detailed size of the enclosure is shown in Figure 3 (a) and (b).

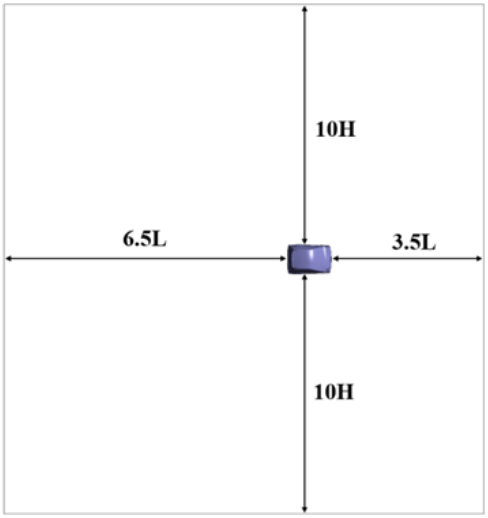


(a)

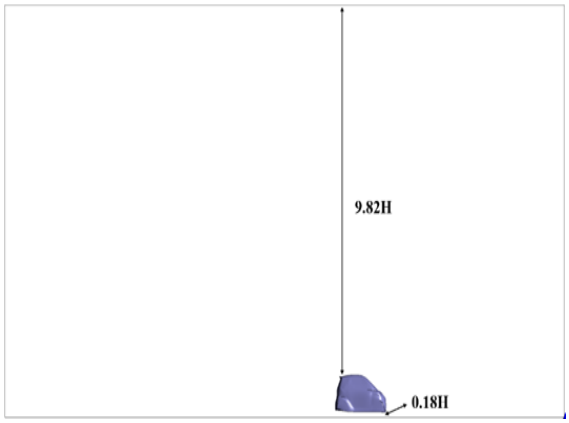


(b)

**Fig. 3: The size of the enclosure [14]**

The following process is the meshing process. The concept of meshing process is where the enclosure and the complicated geometries were split into simple elements. In this stage, the selection of the inlet velocity, outer pressure, ground, vehicle surface, and wall were specified clearly. The smoothing sensitivity of the meshing is set to high. Figure 4 shows the result of the completed meshing.

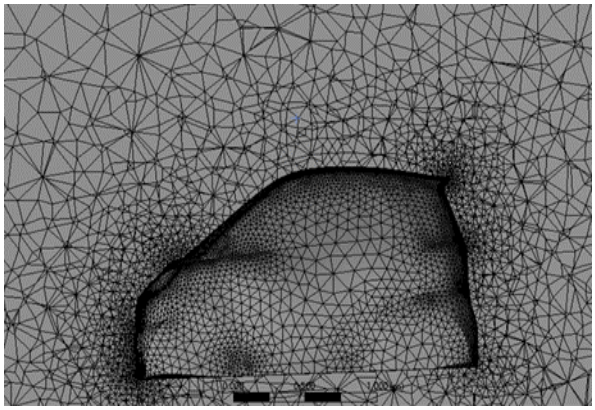

**Fig. 4: Meshing process completed**

After the meshing process had been completed, the model's boundary conditions such as velocity inlet, pressure outlet, vehicle surface, and wall enclosure, turbulence models, hybrid initialization, and the number of iterations must be specified in the setup process as shown in Figure 5. The boundary conditions are applied for the no crosswind and crosswind conditions. After all the boundary conditions, hybrid initialization, and the number of iterations had been specified and set up, the process of simulation can be run and the collect all the data that required and perform the data analysis. The Reynolds number that applies in this study were $2.76\times10^6$ and $7.23\times10^5$ which represents the high and low Reynolds number respectively [16]. Besides, this study had applied the Reynolds-Averaged Navier-Stokes (RANS) with the k - $\varepsilon$ turbulence model. The details of boundary conditions applied can be seen in Table 3.

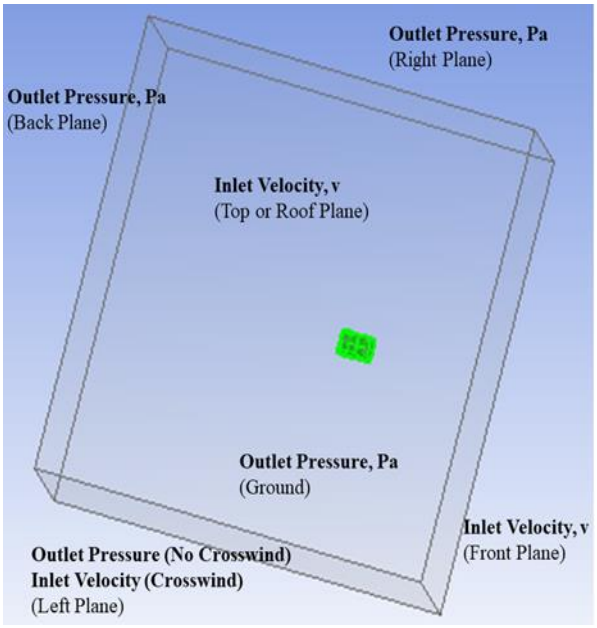


**Fig. 5: Boundary conditions in the numerical analysis [14]**

**Table 3: Boundary conditions**

| Details | Boundary Conditions | Value |
|---|---|---|
| Inlet | Velocity Inlet<br>Crosswind Inlet | 8 m/s and 30 m/s |
| Outlet | Pressure Outlet | 0 Pa (gauge) |
| Wall | Pressure Outlet | 0 Pa (gauge) |
| Vehicle surface | Wall Boundary | No-slip |

## 3. Results and Discussion

### 3.1 Aerodynamics Loads

Figure 6(a) shows the value of drag coefficient against different crosswind conditions for two Reynolds numbers (i.e., 2.76×106 (High Reynolds) and 7.23×105 (Low Reynolds). Based on the observation, both cases of Reynolds numbers acquired a high value for the low range of crosswind conditions i.e., $\Psi \leq 45°$. However, the drag coefficient (Cd) can be described as low in value for a high crosswind condition i.e., $\Psi \geq 60°$. Besides, the trend behaviour of drag coefficient (Cd) for both Reynold numbers outline inconsistency as the crosswind yaw angle increases. At $\Psi = 30°$, the drag coefficient (Cd) for the high Reynold number and low Reynold number is the peak value. Unfortunately, the trend of the drag coefficient decreases drastically from $\Psi = 30°$ to $\Psi = 60°$. Lastly, the trend of the drag coefficient (Cd) had dropped to the lowest at $\Psi = 90°$.

Figure 6(b) reveals the graph behaviour of lift coefficient (Cl) against different crosswind conditions. Generally, both Reynolds numbers (i.e., 2.76×106 (High Reynolds) and 7.23×105 (Low Reynolds) behaved similarly as the crosswind yaw angle got larger. The general trend of lift coefficient (Cl) for both Reynolds numbers shows a steady increase to a maximum value at $\Psi = 90°$. For low crosswind conditions where the range is $\Psi \leq 45°$, the lift coefficient (Cl) is in negative value. The negative value of lift coefficient (Cl) indicated the resultant pressure is pointed downwards. Conversely, for a high crosswind condition where the range is $\Psi > 45°$, the lift coefficient (Cl) is in positive value. The positive value of lift coefficient (Cl) specified that the resultant pressure is pointed upwards. As a result, the entire body of the vehicle model has a role and significant impact in defining the magnitude of lift coefficient (Cl) in this range of crosswind yaw angles.

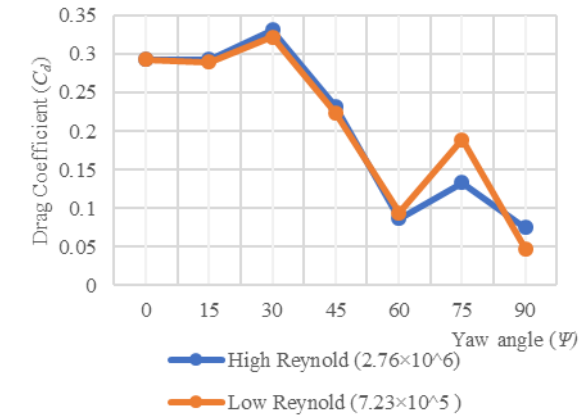


(a)

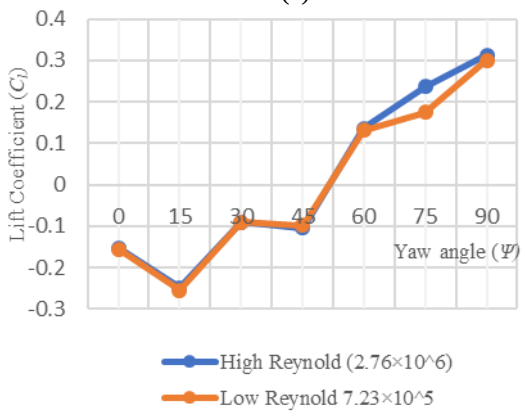


(b)

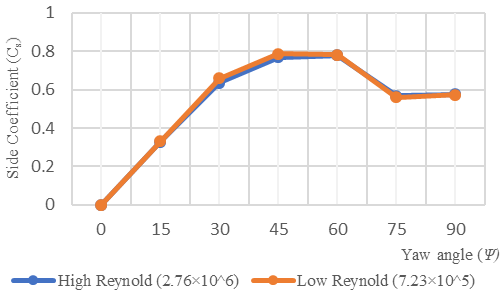


(c)

**Fig. 6: Graph of different aerodynamics loads against different crosswind conditions (a) Drag coefficient (b) Lift coefficient (c) Side coefficient**

One of the factors that cause the vehicle to stray from its course is the side coefficient ($C_s$). In Figure 6(c), as generally, both Reynolds numbers (i.e., $2.76\times10^6$ (High Reynolds) and $7.23\times10^5$ (Low Reynolds) acted in the same way. Furthermore, as the crosswind conditions grow in the range of $0° \leq \Psi \leq 45°$, the side coefficient ($C_s$) displays an increasing pattern. Moreover, it can be observed that the initial point of the side coefficient ($C_s$) is zero. This is due to the flow being symmetrical to the body. Then, the side coefficient ($C_s$) shows a decreasing trend as the crosswind yaw angle gets larger where the range is between $45° \leq \Psi \leq 75°$. Lastly, the side

coefficient ($C_s$) exhibits a modest inclining trend when the crosswind conditions increase from 75° to 90°.

### 3.2 **Vehicle Viewpoint**

The vehicle viewpoint of the velocity streamlines and the pressure contour of the vehicle model is shown in this section. From the top view, the plane formed parallel to the ground, which is sliced through 320mm from the vehicle's bottom surface. From the side view, the plane that formed is parallel to the crosswind inlet surface which is sliced through 798mm from the side of the vehicle as shown in Figure 7(a) and (b). The top and side view will be used to analyze for no crosswind condition while in crosswind condition the top view will be applied. Since there is no significant difference between the high Reynolds and low Reynolds numbers hence the high Reynolds number will be discussed in the following subsection since it is the worst-case condition.

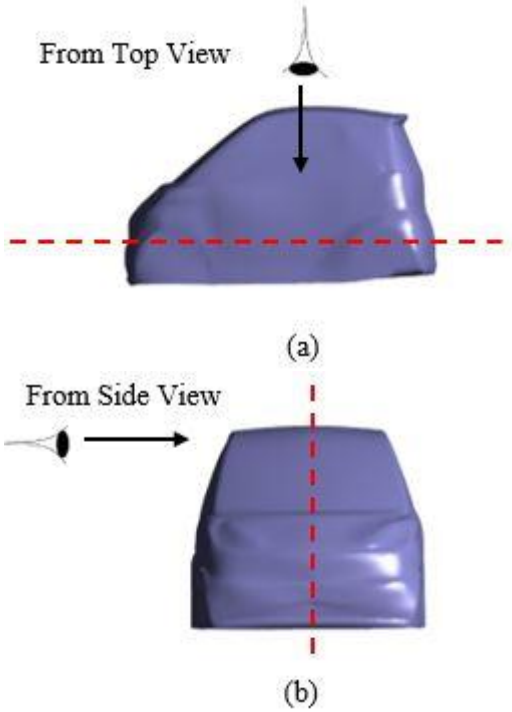


**Fig. 7: Vehicle viewpoint**

### 3.3 **Pressure Contour and Velocity Streamline**

Based on Figure 8(a) which is observed from the top view, the high pressure is located on the vehicle's frontal surface. The low pressure is projected on the front edge of the windward and leeward area. By referring the Figure 8(b) which is observed from the side view, the low pressure occurs at the roof top of the vehicle model. In the perspective of the velocity streamline, based on Figure 8(a), the streamline begins to divide at the frontal surface of the vehicle, which is also known as the stagnation point. The size of the vortices on both sides is equally symmetrical, which clarifies why the side force is zero at this wind condition. In addition, due to flow separation at both sides of the rear edges, two recirculating vortex bubbles are formed at the rear part of the vehicle. From the side view, as shown in Figure 8(b), it also can be visualized that the vortex is formed at the rear side of the vehicle. This is because there is a flow separation occurring at the rear top edge of the vehicle.

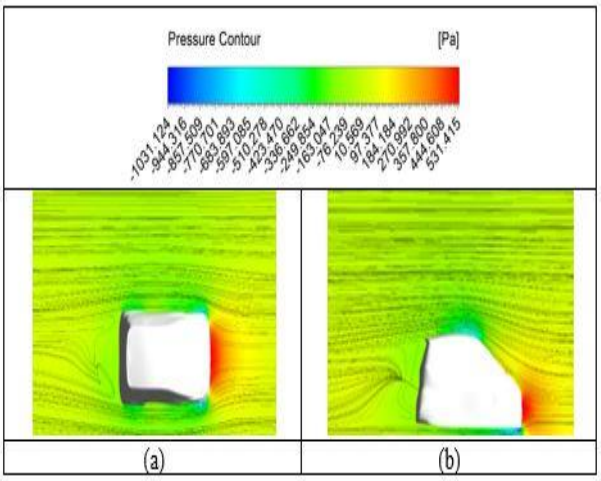


**Fig. 8: Top view and side view of pressure contour superimposed with velocity streamline without crosswind conditions**

At $\Psi$ = 15° which is the crosswind situation, the optimum view to analyze the behaviour is from the top. Based on Figure 9(a), it can be observed that the high-pressure contour had shifted a little right at the frontal surface area of the vehicle compared to $\Psi$ = 0°. However, the low pressure is projected at the front edge of the leeward area. From a velocity streamline standpoint, it can be observed that there is a total of 3 vortex bubbles are formed. The vortex bubbles will form basically due to the separation of flow of the streamline. The location for the flow separation to occur are at the front edge of the leeward area and both rear edge of the vehicle. As a reflection to Figure 6(c) which is the side coefficient ($C_s$), the side coefficient ($C_s$) begins to rise in value. This unbalanced flow scenario is caused by the pressure differential between the leeward and windward zones.

At $\Psi$ = 30° in Figure 9(b), the high-pressure region that had impacted the vehicle frontal area had progressively migrated to the windward side. However, the low pressure is located at the leeward side of the vehicle. In the velocity streamline approach, two vortex bubbles are formed. The location that formed the vortex bubbles is at the area of front edge of the leeward region and rear edge of the windward area. Flow separation at the vehicle leeward leading edge is what causes this enormous recirculating vortex bubble to emerge. In the perspective of aerodynamics load, the increase in the side coefficient ($C_s$) shown in Figure 6(c) implies that the high-pressure region on the windward side is increasing, while the low-pressure region on the leeward side is widening.

At $\Psi$ = 45° in Figure 9(c), the high-pressure region is at the front edge of the windward area. The front edge of the leeward area and the rear edge of the windward area, on the other hand, have a low-pressure region. In the velocity streamline, the recirculating vortex bubble is

formed at the low-pressure zone. Interestingly, there is a need to also mention that the size of the recirculating vortex bubble that forms is out of the ordinary. The size of the vortex bubble that developed should theoretically be a little greater than the vortex bubble that formed at $\Psi$ = 30°, but it does not. The position of the slice across the car model might not be at the correct location to visualise the actual size of vortex formed. The detail of explanation on this part can be referred to in *Sub-chapter 3.5: Vorticity* under the explanation of Figure 11(d). When comparing aerodynamic load factors, however, the side coefficient ($C_s$) in Figure 6(c) has increased slightly due to the pressure differential between the windward and leeward regions. Nevertheless, the parameter of drag coefficient ($C_d$) that had shown in Figure 6(a) had decreased significantly. This is because the drag coefficient ($C_d$) that gives the impact to the vehicle is not critical under the influence of a steady crosswind.

At $\Psi$ = 60°in Figure 9(d), considered as a strong crosswind condition, the high-pressure zone that had impacted the car model had totally shifted to the windward side. The low-pressure area occurred at the front edge of the leeward area and the rear edge of the windward area. From a velocity streamline point of view, it can be observed a massive recirculating vortex bubble is present due to flow separation at the leeward leading edges, and it is practically conquering the area of the leeward region. With further evidence by comparing the aerodynamics load properties where the side coefficient ($C_s$) that present in Figure 6(c) is compared, the value of the side coefficient ($C_s$) is still continuously increasing due to the pressure differences of the windward and leeward area.

At $\Psi$ = 75° in Figure 9(e), the high-pressure region that hit the vehicle model is at windward region and the position had moved to the left a little as compared to $\Psi$ = 60°. However, the low-pressure region presents in four locations which are at the front and rear edge of the windward area as well as the front and rear edge of the leeward area. The low-pressure region that reflects on the front and rear edge of the windward area is more obvious at the $\Psi$ = 75°. In terms of velocity streamline, a total of four recirculating vortex bubbles have been formed. The flow separation that occurred is the main reason that alters the recirculating vortex bubbles to form. Nevertheless, when the side coefficient ($C_s$) that is illustrated in Figure 6(c) is compared, the value of the side coefficient ($C_s$) had dropped significantly compared to $\Psi$ = 60°. Based on one study, the behaviour of the side coefficient ($C_s$) had behaved the same way as the current case where the side coefficient ($C_s$) in that study had dropped slightly in the transition regime as the crosswind yaw increases ($\Psi \geq 75°$).[17]

At $\Psi$ = 90° in Figure 9(f), the high-pressure region projected on the vehicle model is totally at the centre of the windward area. However, the low-pressure region is present on the front and rear edge of the windward area. Moreover, in the perspective of velocity streamline, the streamline begins to divide at the windward surface of the vehicle, where the centre location of the vehicle model in the windward region is also known as the stagnation point. In addition, recirculating vortex bubbles develop entirely on the leeward area due to flow separation at the front and rear edges of the leeward. As compared to $\Psi$ = 75° in terms of side coefficient ($C_s$) that reveal in Figure 6(c), the side coefficient ($C_s$) at $\Psi$ = 90° increased marginally but not as much as the $\Psi$ = 60°. This behaviour had the same attitude as the Ishak *et al.* study where the side coefficient ($C_s$) had dropped slightly in the transition regime as the yaw angle increases ($\Psi \geq 75°$), the value of ($C_s$) becomes more consistent [17].

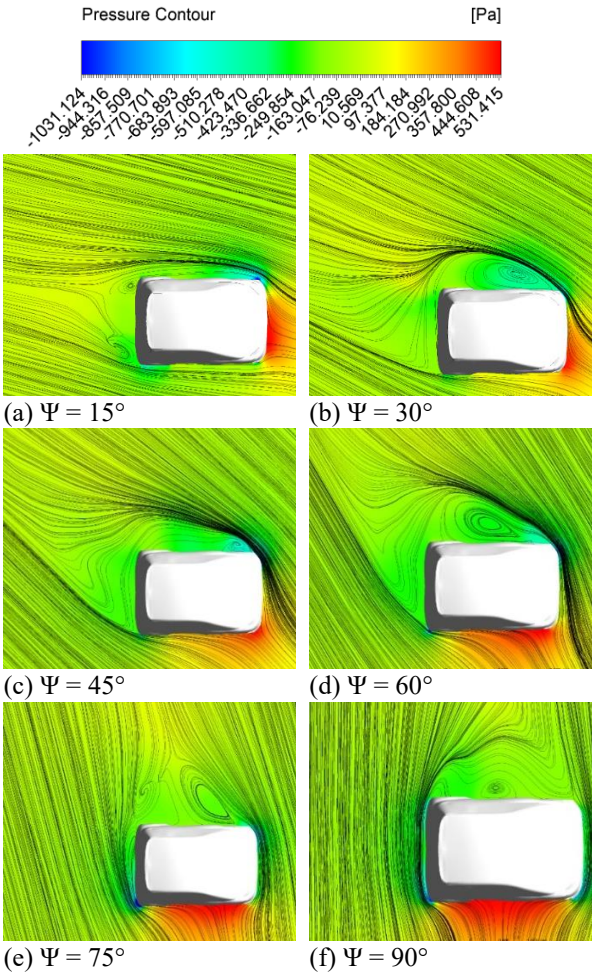


**Fig. 9: Top view and side view of pressure contour superimposed with velocity streamline with crosswind conditions**

3.4 Pressure Contour on Vehicle Surface

At $\Psi$ = 0°, in Figure 10(a), a recirculate region arises under this situation because of flow separation at both front side edges, resulting in low-pressure regions on all surfaces near the leading edges. The size of the generated recirculation region determines the size of the low-pressure region. When the flow reattaches, the pressure on the vehicle surface drops to negative value which is the low-pressure region. The pressure contour on the vehicle surface shifts character as the flow direction increases.

In the case of the $\Psi = 15°$ in Figure 10(b), the low-pressure zone on the windward surface area begins to withdraw and expand to the leeward surface. This is the result of the flow disengaging from the front windward side edges. As it turns out, no low-pressure line is noticed on the vehicle model side edge due to the separation emerging from the front windward leading edge. However, the low-pressure line zone is increasing on the leeward side edge. Apart from that, the high-pressure zone that was exerted on the vehicle's frontal area begins to migrate to the windward side.

The high pressure exerted on the windward surface increases as the crosswind yaw angle increases. Furthermore, the low-pressure line begins to appear at the vehicle rear top and side edge on the windward and at the same time, it also appears at the leeward side edge as the crosswind yaw angle increases. The appearance of the line of the low-pressure zone on the windward and leeward side edges, which depicts the line vortex, indicates that the vortex is just not integrating with the leeward vortices.

On the other hand, at $\Psi = 60°$ that reveals in Figure 10(e), the high pressure exerted on the vehicle frontal surface drops dramatically, and finally being completely covered by the medium pressure region at $\Psi = 75°$ that illustrates in Figure 10(f). Additionally, $\Psi = 60°$, the high-pressure region had been completely displaced to the windward side. In this case, it can cause the vehicle to overturn as it travels, which explains why the lift coefficient ($C_l$) has a positive behaviour as shown in Figure 6(b). On the windward side, when the crosswind yaw angle increases from $\Psi = 60°$ to the maximum of the simulation, which is $\Psi = 90°$ as shown in Figure 10(g), the low-pressure line region becomes larger and slowly expand from the rear side edge to the front side edge of the vehicle. Due to flow separation at the front, rear, and top side edges, the recirculation area forms, resulting in low-pressure regions on all surfaces near the leading edges. The size of the low-pressure region is influenced by the size of the generated recirculation region. The pressure on the vehicle surface reduces to practically zero when the flow reattaches. The low-pressure line region vanishes in the leeward area.

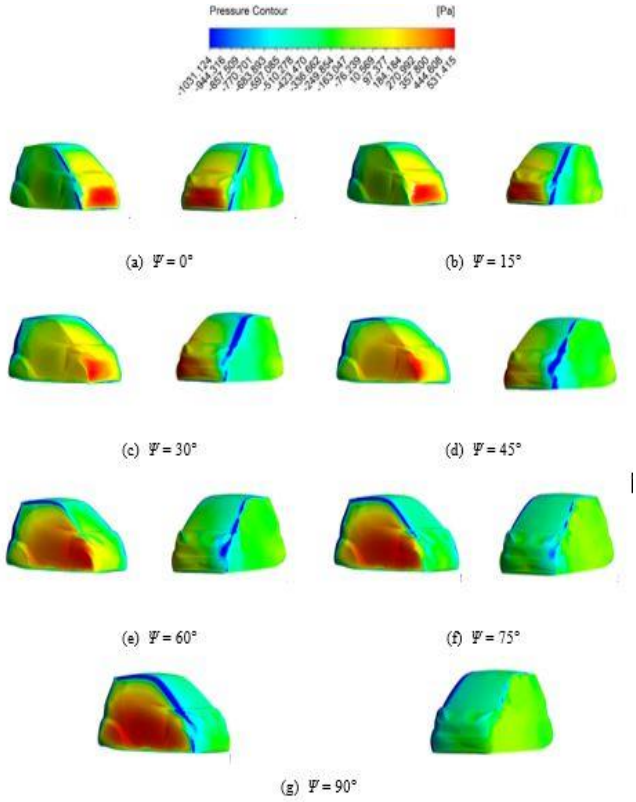


**Fig. 10: Pressure Contour on vehicle surface for different crosswind conditions**

3.5 Vorticity

Figure 11 shows the vortex formation for the vehicle model flow region ($0° \leq \Psi \leq 90°$). At $\Psi = 0°$ in Figure 11(a), the flow separations occur as the flow passes the leading edge, and the vortices form at the area of the rear top edge of the vehicle. Besides, these vortices form symmetrically at both front side edges as well of the model before the flow reattaches. When the direction of the flow increases to $\Psi = 15°$ in Figure 11(b) vortices start to appear on the leeward area and the rear side of the vehicle following the wind direction. Flow separation at the leeward edge from the frontal surface of the vehicle surface causes a more noticeable path of the vortex. In the wake flow, this vortex is in the leeward lower half end of the recirculation region. Additionally, a new cylindrical vortex is formed and is also known as the recirculation region in the wake flow. The splitting of the flow after passing the rear edge of the vehicle model causes this condition.

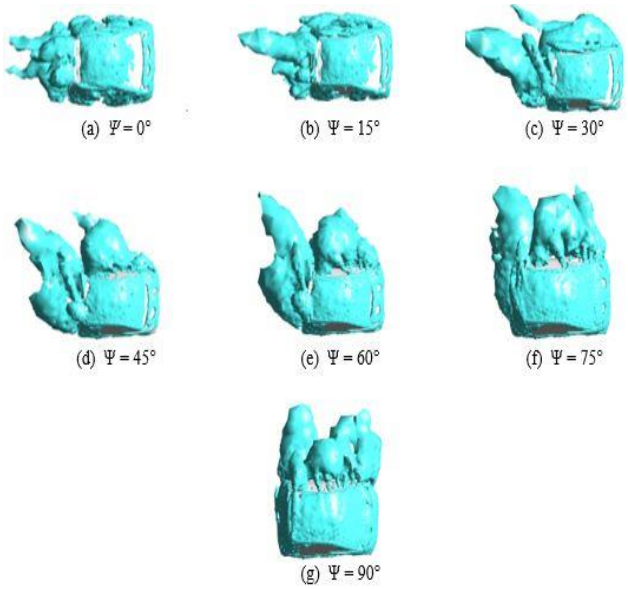


**Fig. 11: Vorticity behaviour around the vehicle for different crosswind conditions**

The route of vortices diverges in the direction of the flow direction as the wind flow direction increases to $\Psi$ = 30° in Figure 11(c). Two vortex forms at the side edge of the leeward area, and it is more visible than the $\Psi$ = 15°. Furthermore, a new vortex bubble is generated along the leeward region, and a big recirculation region of the wake flow is formed at the rear end of the vehicle model under this yaw angle condition. This occurrence is anticipated, as it will occur on a regular basis after each other sheds away in its prior path. A similar observation is made with respect to the route of vortices that begins to disengage further from the leeward surface as the flow yaw angle increases.

Impressively, at $\Psi$ = 45° in Figure 11(d), it can be discovered that a total of two vortex bubbles and two recirculation regions of the wake flow are from, with two recirculation regions of the wake flow forming on the vehicle rear side and the other two vortex bubbles forming on the vehicle leeward side. The vortex bubbles that developed are larger and diverge more than the vortex bubbles that formed at Ψ = 30°. Aside from that, based on the velocity streamline behaviour in Figure 9(c), only one vortex was produced, but when compared to the vorticity characteristic, another large velocity vortex streamline should arise on the leeward region eventually. The position of the plane that slices through the vehicle body is not exact, which explains why the velocity vortex streamline does not emerge in the leeward zone. Moreover, at $\Psi$= 60° as revealed in Figure 11(e), a similar observation that could be described at the $\Psi$ = 45°. In comparison to the $\Psi$ = 45°, the course of recirculation region of the wake flow vortices and the size of the vortex bubbles formed at the $\Psi$ = 60°, is more deviating and greater towards the leeward side.

When the crosswind condition is increased to a value of $\Psi$ = 75° in Figure 11(f), the flow pattern's features alter dramatically. Most of the vortices have developed in the leeward area at this yaw angle, and the top windward edge has progressively evolved into the front leading edge, separating the edges. Furthermore, the path of vortices cannot be recognised clearly as the dominating path at this point, resulting in three enormous vortex bubbles appearing on the leeward area. Finally, at $\Psi$ = 90°, the combined path of vortices generates a wake on the vehicle leeward in Figure 11(g). The windward edge has completely converted into the front leading edge at this point, causing the flow to reflect vehicle body flow behavior.

## 4. Conclusion

The relevance of studying the aerodynamics of a small car vehicle under the influence of a steady crosswind was demonstrated in this Computational Fluid Dynamics (CFD) study. In the aspect of crosswind, all aerodynamic characteristics inclusive the qualitative and quantitative analysis exerts a significant influence on the vehicle dynamic behaviour. Firstly, the crosswind yaw angle has a significant impact on the aerodynamics loads. The parameter that causes this result is the drag coefficient ($C_d$), lift coefficient ($C_l$), and side coefficient ($C_s$). In terms of drag coefficient ($C_d$), at the crosswind yaw angle of $30° \leq \Psi \leq 60°$ it can be concluded that there is a substantial or crucial drop in the range. This is because when the crosswind yaw angle increases, the drag force that hits the vehicle's frontal surface decreases. In the perspective of lift coefficient ($C_l$), it can be deduced that the value is increasing because of the crosswind hitting the vehicle model, which causes it to slowly migrate to the windward side. As this occurs, the overturning of the vehicle becomes more favourable. The conclusion that can be drawn from the side coefficient ($C_s$) is that there is a slight drop in case $\Psi$ = 60° and this result eventually match with the case as in Ishak *et al.* study [17]. Lastly, by comparing the behaviour of low and high Reynold numbers, it can be inferred that there is little variation in aerodynamic load qualities and that they eventually behave the same manner.

Secondly, in terms of the qualitative analysis, the conclusion that could be made for the pressure contour was that as the crosswind yaw angles increases, the high-pressure region that reflected on the vehicle surface was slowly migrated to the windward area. The low-pressure area, on the other hand, projected onto the vehicle's edge. From the standpoint of the velocity streamline, it can be stated that the streamline begins to separate or divide when it meets the vehicle's surface, which is referred to as the stagnation point. As the crosswind yaw angle increased, the vortex bubble streamline grew larger. Besides, the aberrant production of vortex bubbles observed when $\Psi$ = 45° can be attributed to an inaccuracy in slicing position through the vehicle model. In the context of pressure contour that reflected on vehicle surface, the conclusion that can be drawn was the low-pressure region will be present on the leeward edge of the vehicle as the crosswind yaw angles increases. When the crosswind yaw angle goes is beyond $\Psi \geq 60°$, the low-pressure region slowly disappears on the edge of the

leeward and formed on the edge of the windward. Nevertheless, the high-pressure region will be reflected on the frontal surface of the vehicle. As the crosswind yaw angle increases, the high-pressure region progressively migrates to the windward area. In terms of vorticity, when crosswind yaw angles increase, the tendency for the creation of vortex bubbles increases as well. As a reflection to the case in $\Psi = 45°$, it had been proven that a massive vortex bubble has generated in the leeward area. The research objectives had successfully achieved.

**Acknowledgement**

The authors would like to thank the Ministry of Higher Education (MOHE) for supporting this research under the Fundamental Research Grant Scheme No. Vot K333 and Research Fund Universiti Tun Hussein Onn Malaysia (H725).

**References**

[1] S. Indexed, S. Agarwal, and U. Pradesh, "Aerodynamics of vehicles," vol. 11, no. 11, pp. 1996–2001, 2020, doi: 10.34218/IJARET.11.11.2020.

[2] Z. M. Jawi, R. Sarani, W. S. Voon, A. Farhan, and M. Sadullah, *Weather as a Road Safety Hazard in Malaysia - An Overview*, no. May. Selangor: Malaysian Institute of Road Safety Research (MIROS), 2009.

[3] S. A. Coleman and C. J. Baker, "An experimental study of the aerodynamic behaviour of high sided lorries in cross winds," *J. Wind Eng. Ind. Aerodyn.*, vol. 53, no. 3, pp. 401–429, 1994, doi: 10.1016/0167-6105(94)90093-0.

[4] Q. Zhang, C. Su, and Y. Wang, "Numerical Investigation on Aerodynamic Performance and Stability of a Sedan Under Wind–Bridge–Tunnel Road Condition," *Alexandria Eng. J.*, vol. 59, no. 5, pp. 3963–3980, 2020, doi: 10.1016/j.aej.2020.07.004.

[5] D. McArthur, D. Burton, M. Thompson, and J. Sheridan, "An experimental characterisation of the wake of a detailed heavy vehicle in cross-wind," J. Wind Eng. Ind. Aerodyn., vol. 175, no. January, pp. 364–375, 2018, doi: 10.1016/j.jweia.2018.01.033.

[6] T. Tunay, E. Firat, and B. Sahin, "Experimental investigation of the flow around a simplified ground vehicle under effects of the steady crosswind," *Int. J. Heat Fluid Flow*, vol. 71, no. December 2017, pp. 137–152, 2018, doi: 10.1016/j.ijheatfluidflow.2018.03.020.

[7] S. D. Kwon, D. H. Kim, S. H. Lee, and H. S. Song, "Design criteria of wind barriers for traffic. Part 1: Wind barrier performance," *Wind Struct. An Int. J.*, vol. 14, no. 1, pp. 55–70, 2011, doi: 10.12989/was.2011.14.1.055.

[8] I. Bayraktar, D. Landman, and O. Baysal, "Experimental and computational investigation of Ahmed body for ground vehicle aerodynamics," *SAE Tech. Pap.*, no. 724, 2001, doi: 10.4271/2001-01-2742.

[9] F. J. Bello-Millán, T. Mäkelä, L. Parras, C. del Pino, and C. Ferrera, "Experimental study on Ahmed's body drag coefficient for different yaw angles," *J. Wind Eng. Ind. Aerodyn.*, vol. 157, pp. 140–144, 2016, doi: 10.1016/j.jweia.2016.08.005.

[10] J. Keogh, T. Barber, S. Diasinos, and D. Graham, "The aerodynamic effects on a cornering Ahmed body," *J. Wind Eng. Ind. Aerodyn.*, vol. 154, pp. 34–46, 2016, doi: 10.1016/j.jweia.2016.04.002.

[11] W. Meile, T. Ladinek, G. Brenn, A. Reppenhagen, and A. Fuchs, "Non-symmetric bi-stable flow around the Ahmed body," *Int. J. Heat Fluid Flow*, vol. 57, pp. 34–47, 2016, doi: 10.1016/j.ijheatfluidflow.2015.11.002.

[12] Z. M. Saleh and A. H. Ali, "Numerical Investigation of Drag Reduction Techniques in a Car Model," IOP Conf. Ser. Mater. Sci. Eng., vol. 671, no. 1, pp. 1–15, 2020, doi: 10.1088/1757-899X/671/1/012160.

[13] Y. E. William, "Investigation of Crosswind Aerodynamics for Road," *Elev. Int. Conf. Fluid Dyn.*, no. December 2014, pp. 1–11, 2013, doi: 10.13140/2.1.2297.5048.

[14] T. Favre, "Aerodynamics simulations of ground vehicles in unsteady crosswind," PhD thesis, KTH Stock., 2011.

[15] Q.-L. WANG, Z. WU, X.-L. ZHU, L.-L. LIU, and Y.-C. ZHANG, "Analysis of Aerodynamic Performance of Tesla Model S by CFD," *Adv. Eng. Res.*, vol. 131, no. Eeeis, pp. 16–21, 2017, doi: 10.2991/eeeis-17.2017.3

[16] A. Bornioli, I. Bray, P. Pilkington, and J. Parkin, "Effects of city-wide 20 mph (30km/hour) speed limits on road injuries in Bristol, UK," *Inj. Prev.*, vol. 26, no. 1, pp. 85–88, 2020, doi: 10.1136/injuryprev-2019-043305.

[17] I. A. Ishak, "The Flow Behaviour Around a Generic Train Moving on Different Infrastructures under the Influence of Crosswind," Univ. Teknol. Malaysia, p. 236, 2018.